ORIGINAL ARTICLE

Biodistribution and PET imaging of [18F]FMISO in mousecolon cancer xenografted mice

Sudhakara Reddy Seelam[1,2,3], Ji Youn Lee[1,2,3], Young Joo Kim[1,2], Yun-Sang Lee[1,2,3], and Jae Min Jeong[1,2,3,*]

[1]Department of Nuclear Medicine, Institute of Radiation Medicine, Seoul National University College of Medicine, Seoul, Korea;
[2]Cancer Research Institute, Seoul National University College of Medicine, Seoul, Korea;
[3]Department of Radiation Applied Life Science, Seoul National University College of Medicine, Seoul, Korea

ABSTRACT

Hypoxia is an important adverse prognostic factor for tumor progression and is a major cause of failure of radiation therapy. In case of short-term hypoxia, the metabolism can recover to normal, but if hypoxia persists, it causes irreversible cell damage and finally leads to death. So a hypoxia marker would be very useful in oncology. In particular, 2-nitroimidazole can be reduced to form a reactive chemical species, which can bind irreversibly to cell components in the absence of sufficient oxygen, thus, the development of radiolabeled nitroimidazole derivatives for the imaging of hypoxia remains an active field of research to improve cancer therapy result. 2-nitroimidazole based hypoxia marker, [18F]FMISO holds promise for the evaluation of tumor hypoxia by Positron emission tomography (PET), at both global and local levels. In the present study, [18F]FMISO was synthesized using an automatic synthesis module with high radiochemical purity (>99%) in 60 min. Immunohistochemical analysis using pimonidazole confirmed the presence of hypoxia in xenografted CT-26 tumor tissue. A biodistribution study in CT-26 xenografted mice showed that the increased tumor-to-muscle ratio and tumor-to-blood ratios from 10 to 120 min post-injection. In the PET study, [18F]FMISO also showed increased tumor-to-muscle ratios from 10 to 120 min post-injection. In conclusion, this study demonstrates the feasibility and utility of [18F]FMISO for imaging hypoxia in mouse colon cancer model using small animal PET. *J Radiopharm Mol Probes 1(2):137-144, 2015*

Key Words: [18F]FMISO, PET, Fluorine-18, Hypoxia, CT-26 mouse colon cancer

Introduction

Positron emission tomography (PET) is an important imaging modality to evaluate neurologic, oncologic and cardiologic abnormalities (1-7). ^{18}F ($t_{1/2}$ = 109.77 min, 90% β+, $E_{\beta+max}$ = 0.635 MeV, 3% EC) is the most commonly used PET radioisotope because of excellent imaging properties, and thus, the development of ^{18}F-labeled bioactive molecules has become an important area.

Various ^{18}F-labeled 2-nitroimidazole derivatives such as [18F]fluoromisonidazole ([18F]FMISO, Figure 1) (8,9), [18F]fluoroerythronitroimidazole ([18F]FETNIM) (10), 1-R-D-(2-deoxy-2-[18F]fluoroarabinofuranosyl)-2-nitroimidazole ([18F]FAZA) (11), 2-(2-nitroimidazol-1-yl)-*N*-(3,3,3-[18F]-trifluoropropyl)acetamide, ([18F]EF-3) (12), 2-(2-nitro-1H-imidazol-1-yl)-N-(2,2,3,3,3-[18F]-pentafluoropropyl)acetamide ([18F]EF-5) (13), and 3-[18F]fluoro-2-(4-((2-nitro-1*H*-imidazol-1-yl)methyl)-1*H*-1,2,3,-triazol-1-yl)-propan-1-ol ([18F]HX-4) (14), have been extensively studied to detect tumor hypoxia, because nitroimidazole residue is reduced to reactive chemical species which can bind to cell components in the absence of sufficient oxygen (11,15-20). Among them, [18F]fluoromisonidazole
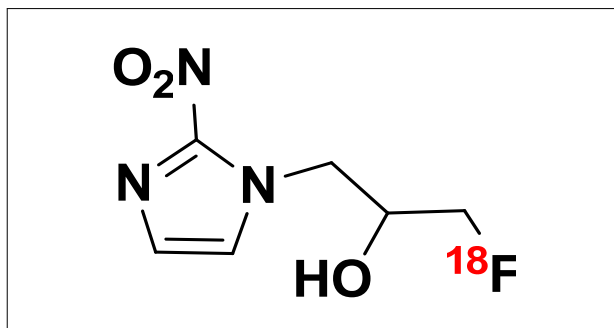
Figure 1: Structure of 1-(2-Nitro-imidazolyl)-3-[18F]fluoro-2-propanol ([18F]FMISO).

([18F]FMISO) is the most widely used nitroimidazole derivative to determine tumor hypoxia *in vivo* for clinical PET (21,22). [18F]FMISO has been shown to selectively bind to hypoxic cells both *in vitro* and *in vivo*. It is used to quantitatively assess tumor hypoxia in the lung, brain, head-and-neck cancer patients (23, 24), and in the hearts of myocardial ischemia patients (25,26). [18F]FMISO has favorable chemical and physicochemical properties in terms of lipophilicity (octanol/water partition coefficient; log P = 2.6) (27) and an appropriate reduction potential of E -389 mV (28) that are responsible for a high cellular uptake and trapping in hypoxic cells.

In the present study, we tried the immunohistochemistry using pimonidazole hydrochloride, to confirm the presence of hypoxia, biodistribution and PET imaging of [18F]FMISO in CT-26 (mouse colon cancer) xenographted mice models at 10, 30, 60, and 120 min post-injection.

Materials and Methods

1. General

[18F] was produced using the [18O] (p,n) [18F] reaction using [18O]-enriched (95%) water by a cyclotron (CYCLONE 18/9 , Ion Beam Applications (IBA), Louvain-la-Neuve, Belgium). FASTlab multi-Tracer disposable cassette (GE Healthcare, Princeton, NJ, USA) was used for the preparation of [18F]FMISO. Radio analytical HPLC was performed using a XTerra RP18 (4.5×100 mm) columns from Waters Corporation (Milford, MA, USA) to confirm the radiochemical purity. The solvent systems used were A (0.1% TFA in H_2O), B (MeCN) and the flow rate for analytical HPLC was 1 mL/min (95% of B with 5% of A for 13 min). The gamma scintillation counter was a Packard Cobra II (Global Market Institute, MN, USA). PET images were obtained using a small-animal PET scanner from GE Healthcare

(Princeton, NJ, USA). The animal studies were performed in Seoul National University Hospital, Seoul, Korea, which is fully accredited by AAALAC International (2007, Association for Assessment and Accreditation of Laboratory Animal Care International).

2. Immunohistochemical analysis

Hypoxyprobe™-1 (pimonidazole hydrochloride, 60 mg/kg) was diluted in 150 μL of PBS and intravenously injected into each CT-26 xenografted mouse (n = 3). Mice were sacrificed at 90 min post-injection. The tumor was isolated and directly frozen in liquid nitrogen until cryosectioning into 7-μm thin slices using a Leica CM1800 Cryostat (IMEB Inc., CA, USA). The sections were then stored at -80°C until staining. The fixed tumor sections were washed with phosphate buffered saline (PBS) containing 0.2% Brij 35 and exposed to 3% hydrogen peroxide for 5 min at room temperature to quench endogenous peroxidase activity. The sections were incubated with a protein-blocking agent for 5 min at room temperature to minimize nonspecific binding. The samples were incubated for 60 min at room temperature with mouse monoclonal anti-pimonidazole antibody (MAb1) diluted in PBS, and washed. Samples were incubated with a secondary biotinylated antibody, and with a biotin-streptavidin-peroxidase complex, and, finally, with 3,3′-diaminobenzidine (DAB), which imparts a clear brown color to the marker-antibody complex around the nucleus of the hypoxic cells. Between all steps of the staining procedure, the sections were rinsed three times with PBS containing 0.2% Brij 35 for 2 min at 0°C. Finally, the sections were mounted with CC/Mount from Sigma-Aldrich (St. Louis, MO, USA). The cells and histological sections were viewed with a microscope (Olympus America Inc., Melville, NY, USA) to investigate whether they were stained brown, indicating hypoxia.

3. Biodistribution study using colon cancer xenograft mice

CT-26 cells cultured in DMEM containing 10% fetal bovine serum were harvested after treatment with 0.05% trypsin. Cells were washed with 10 mL of PBS by centrifugation (3,000 rpm). Each BALB/c mouse was subcutaneously injected with 2 × 10^5/0.1 mL CT-26 cells in the right shoulder. After 2 weeks, [18F]FMISO (0.15 MBq/ 0.1 mL) were intravenously injected into each xenografted mouse (n = 4). Mice were sacrificed at 10, 30, 60, and 120 min post-injection. Tumor, blood, muscle, and

other organs were separated immediately, and their weights and radioactivity values were obtained using a balance and a γ-scintillation counter, respectively. Results are expressed as the percentage of injected dose per gram of tissue (% ID/g).

4. PET of tumor-bearing mice

CT-26 cells ($2×10^5$ cells) in normal saline (0.1 mL) were subcutaneously injected into the right shoulders of the mice and grown for 14 days to produce tumors of ~16 mm in diameter. [^{18}F]FMISO (1.85 MBq/0.1 mL) was intravenously injected through the tail vein. The mice were anesthetized with 2% isoflurane by inhalation and PET images were obtained at 10, 30, 60, and 120 min post-injection. PET studies were performed using a dedicated small-animal PET scanner. Emission data were acquired for 10 min. The three-dimensional raw emissions data were reconstructed to temporally framed sinograms by Fourier rebinning, using an ordered subset expectation maximization (OS-EM) reconstruction algorithm attenuation correction. For the PET images, data from 10 frames were analyzed (10 times with 1-min frames).

5. Data analysis

The software AsiPro VM 5.0 from Concorde Inc. (Knoxville, TN, USA) was used to process images. To assess uptake of the labeled derivatives by tumors cells, circular regions of interests (ROI) were placed (1.5-mm radius) at locations of maximum tracer uptake in tumors and in muscles as references. Relative tracer uptake was expressed as the ratio of tumor to muscle counts. Having placed ROIs, standard uptake values (SUVs) were calculated using the equation SUV=CCF/(injected dose/body weight of mouse). The CCF (decay-corrected activity concentration) was calculated using the equation CCF (MBq/mL) = radioactivity (mCi/mL) × branching ratio × ROI (value/pixel); the branching ratio of ^{18}F is 0.967.

Results and Discussion

1. Synthesis of [^{18}F]FMISO

To synthesize the [^{18}F]FMISO, (2′-Nitro-1′-imidazolyl) -2-O-acetyl-3-O-tosylpropanol, precursor was used. A TracerLab Mx disposable cassette from GE Healthcare Technologies was used for the production of [^{18}F]FMISO (29). The radiochemical purity of the prepared [^{18}F]FMISO was greater than 99% by radio-HPLC (Figure 2). Decay-corrected radiochemical yield was 50.4±2.8%. The specific activity of the [^{18}F]FMISO is 337±25 GBq/μmol (29)

2. Immunohistochemistry

The existence of hypoxia in the CT-26 xenografted tumor tissue was confirmed by immunohistochemical analysis using a
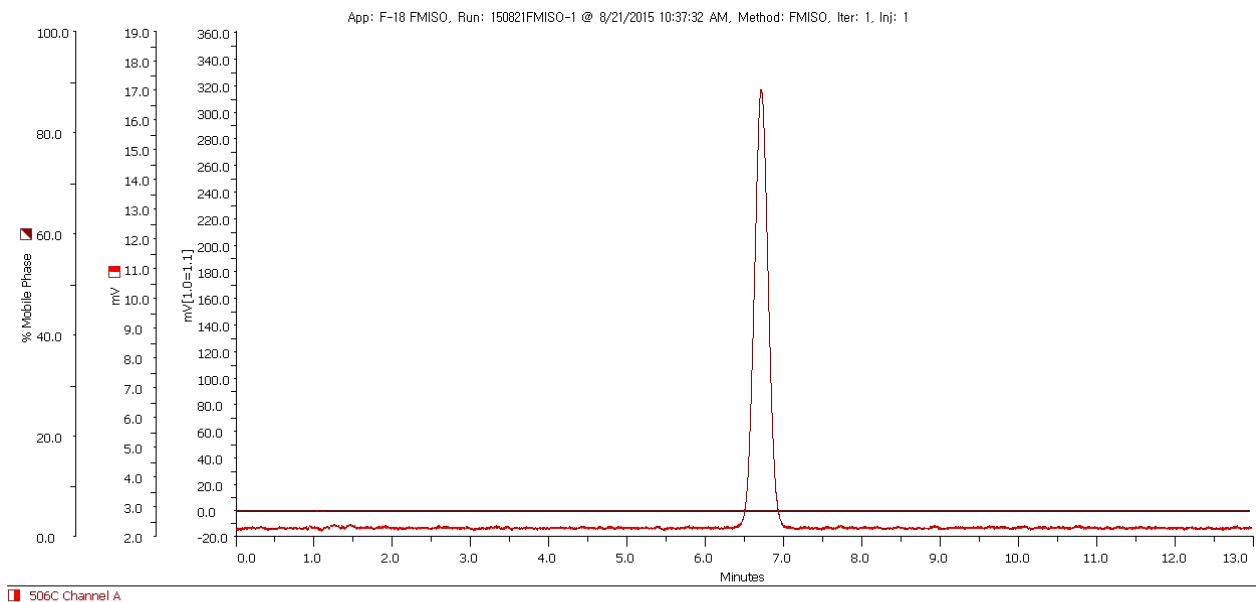

App: F-18 FMISO, Run: 150821FMISO-1 @ 8/21/2015 10:37:32 AM, Method: FMISO, Iter: 1, Inj: 1

506C Channel A

Figure 2. Analytical HPLC chromatogram for quality control of [^{18}F]FMISO eluted at 8.17 min. Red line: radioactive trace.
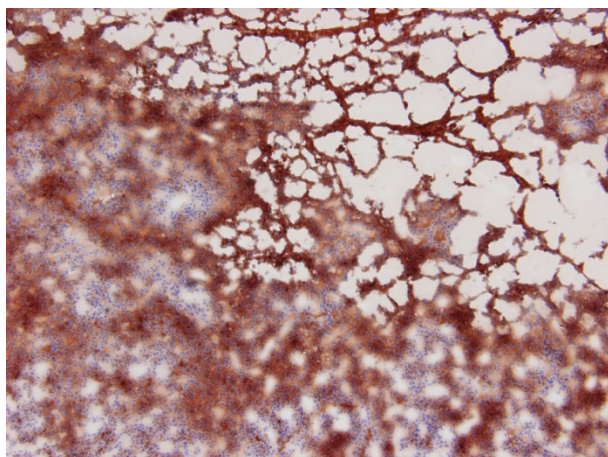
Figure 3. Immunohistochemical staining of CT26 tumor xenografts to detect hypoxia. Tumor tissue was obtained from xenografted mice at 90 min post-injection of pimonidazole hydrochloride. Hypoxic lesions are shown in brown. 40× magnification image.

standard exogenous hypoxia marker, pimonidazole. Pimonidazole hydrochloride was injected into CT-26 xenografted mice via the tail vein. The mice were sacrificed at 90 min post-injection. The tumors were dissected and cut into 7-μm slices at -20°C, and stored at -80°C. To visualize the hypoxic regions, part of the tumor tissue was fixed on the slide and washed. Slides were blocked, incubated with a primary antibody, mouse IgG monoclonal antibody (MAb1) diluted in PBS, washed, and a secondary biotinylated goat-anti-mouse IgG antibody was applied. The biotin-streptavidin peroxidase complex method was used and staining was visualized using the DAB chromophore. Immunohistochemical staining (brown) revealed the presence of hypoxic areas (Figure 3).

3. Biodistribution in xenografted mice

A biodistribution study was performed using mouse colon cancer CT-26 xenografted BALB/c mice after injection of [18F]FMISO (0.15 MBq/ 0.1 mL) via the tail vein (Figure 4A). Mice were sacrificed at 10, 30, 60, and 120 min post-injection. Among the organs evaluated, higher uptake of [18F]FMISO in intestine (10 min: 6.98±0.28; 30 min: 10.15±0.64; 60 min: 12.38±2.00; and 120 min: 11.25±0.93 % ID/g) and liver (10 min: 10.16±0.34; 30 min: 10.53±0.57; 60 min: 8.78±1.57; and 120 min: 6.82±0.21% ID/g) were observed in this study. Large amount of anaerobic bacteria present in the large intestine may account for intestinal uptake, and liver uptake was due to the lipophilicity of [18F]FMISO as mentioned in the literature (11).

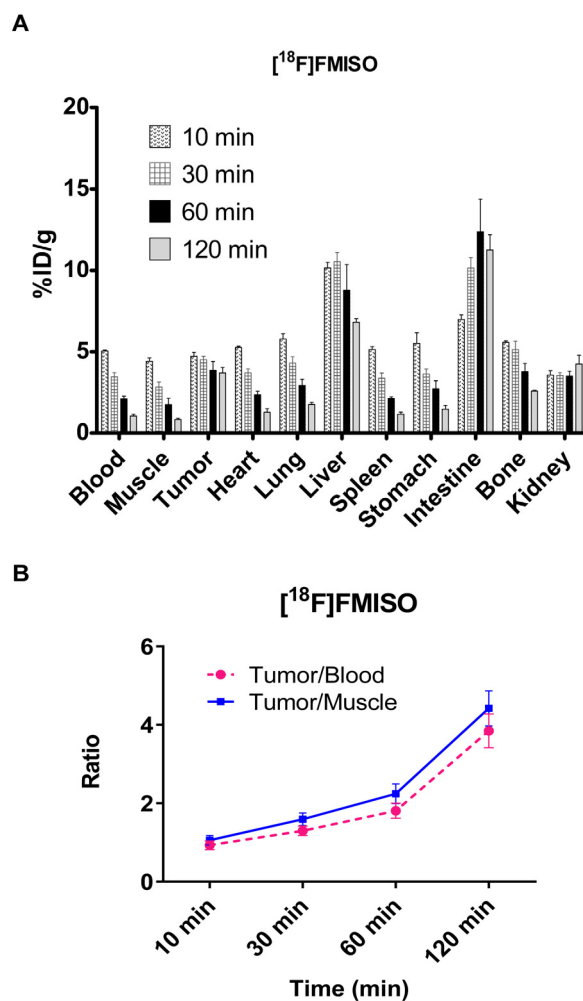**Figure 4.** Biodistribution of (A) [18F]FMISO (0.15 MBq/ 0.1 mL) in CT-26 xenografted mice after 10, 30, 60 and 120min post-injection. (B) Tumor to blood and tumor to muscle ratio with respect to time. Results are mean percentage of injected dose per gram of tissue ± standard deviation (% ID/g ± SD); n = 4 at each time point.

Earlier studies also showed high liver and intestine uptake for [18F]FMISO in AR42J rat pancreatic acinar carcinoma xenografted BALB/c mice (30), EMT6 mouse mammary carcinoma xenografted BALB/c mice (30) and A431 human epidermoid carcinoma xenografted BALB/c mice (30).

For [18F]FMISO, the radioactivity in blood (10 min: 5.05±0.05; 30 min: 3.46±0.26; 60 min: 2.11±0.17; and 120 min: 1.05±0.11 % ID/g) and muscle (10 min: 4.42±0.19; 30 min: 2.84±0.30; 60 min: 1.74±0.41; and 120 min: 0.84±0.08% ID/g) were decreased from 10 to 120 min post-injection (Figure 4A). [18F]FMISO accumulation in heart, lung, spleen, stomach, kidney and bone showed a decreased distribution profile as in blood from 10 to 120 min post-injection (Figure 4A).

Table 1. Comparison of major parameters (%ID/g, T/B, and T/M) of [^{18}F]FMISO in other preclinical studies

Animal	Tumor type	% ID/g	T/B	T/M	Refs.
FMISO					
BALB/c nude mice	A549 human NSCLC			3.5	[34]
BALB/c nude mice	NCI-H520 human NSCLC			4.45	[34]
BALB/c nude mice	NCI-H596 human NSCLC			2.59	[34]
BALB/c nude mice	U87 MG human glioblastoma			1.93	[34]
BALB/c nude mice	PC3 human prostate			3.53	[34]
BALB/c nude mice	DU145 human prostate			2.27	[34]
BALB/c nude mice	Caki human RCC			1.28	[34]
BALB/c nude mice	SK-N-BE human neuroblastoma			2.48	[34]
BALB/c nude mice	CLS-2 human urinary bladder carcinoma			3.62	[34]
BALB/c nude mice	KB-31 human nasopharyngeal carcinoma			5.7	[34]
Swiss nude mice	A431 human epidermoid carcinoma	3.67 (3 h)	4.92 (3 h)	3.95 (3 h)	[35]
BALB/c	B16 mouse melanoma			2.04 (1.5 h)	[34]
Swiss nude mice	AR42J rat pancreatic acinar carcinoma	2.27 (3 h)	3.39 (3 h)	2.92 (3 h)	[35]
BALB/c mice	EMT6 mouse mammary carcinoma	4.32 (3 h)	3.03 (3 h)	3.22 (3 h)	[35]
CDF1 mice	C3H mouse mammary carcinoma	5.38 (2 h)	4.3 (2 h)	6.4 (2 h)	[36]
Copenhagen rats	Dunning rat R3327-AT prostate carcinoma	0.3 (2 h)			[37]
C3H mice	SCCVII mouse squamous cell carcinoma	1.5 (80 min)			[30, 38]
C3H mice	KHT mouse sarcoma	2.24 (4 h)		6.79 (4 h)	[39]
Wistar rats	C6 rat glioma	0.42 (2 h)		2.6 (2 h)	[40]
Wistar rats	Walker 256 rat carcinosarcoma	1.00 (3 h)		2.7 (1 h), 4.4 (3 h)	[11]
Nude rats	Morris rat McA-R-7777 hepatoma	0.72 (3 h)		2.5 (3 h)	[41]

The persistent tumor uptake of the [^{18}F]FMISO (10 min: 4.72±0.25; 30 min: 4.51±0.21; 60 min: 3.85±0.56; and 120 min: 3.70±0.34% ID/g) evidences that [^{18}F]FMISO was bound to intracellular proteins after the hypoxia-sensitive reduction of the nitro moiety to amine (15). The mean tumor uptake values of [^{18}F]FMISO was higher than Al^{18}F-NODA-ethyl-NI (10 min: 2.13 ± 0.41; 60 min: 0.24 ± 0.03; and 120 min: 0.23 ± 0.05 % ID/g) and Al^{18}F -NODA-propyl-NI (10 min: 1.92 ± 0.12; 60 min: 0.33 ± 0.05; and 120 min: 0.22 ± 0.04 % ID/g) (31). The increased tumor-to-blood uptake ratios (10 min: 0.93±0.04; 30 min: 1.30±0.05; 60 min: 1.81±0.19; and 120 min: 3.85±0. 43) and tumor-to-muscle ratios (10 min: 1.06±0.05; 30 min: 1.59±0.11; 60 min: 2.24±0.25; and 120 min: 4.42±0.50) were observed from 10 to 120 min post-injection (Figure 4B). Initial tumor-to-blood and tumor-to-muscle ratios were low, over time [^{18}F]FMISO was gradually cleared from non target tissues, while counts in tumors remained constant. Thus, tumor-to-blood and tumor-to-muscle ratios increased with time (Figure 4B). The comparison of major parameters like % ID/g, tumor-to-blood (T/B), and tumor-to-muscle (T/M) ratios of [^{18}F]FMISO in other studies are shown in Table 1.

4. Mouse PET imaging

A small animal PET study was performed using CT-26 xenografted BALB/c mice. Images were obtained at 10, 30, 60, and 120 min after intravenous injection of [^{18}F]FMISO (1.85 MBq/0.1 mL) via the tail vein (Figure 5). As predicted from the biodistribution study high intestine and liver uptakes were observed for [^{18}F]FMISO. Standardized uptake values (SUVs) were calculated, using the PET images. The [^{18}F]FMISO activity in the muscle, liver and intestines were decreased from 10 to 120 min post-injection (Figure 5).The SUVs of the [^{18}F]FMISO (10 min: 0.18 ± 0.04; 30 min: 0.21 ± 0.02; 60 min: 0.23 ± 0.06; and 120 min: 0.34 ± 0.04) showed the increased uptake from 10 to 120 min post-injection. Because of the low background activity of [^{18}F]FMISO in muscle, [^{18}F]FMISO uptake within the tumor area was low but could be differentiated from the normal muscle and other organs easily at 120 min post-injection. Heterogeneous patterns of accumulation of [^{18}F]FMISO was observed in this study. Similar heterogeneous uptake patterns were previously observed for [^{18}F]FMISO in the syngeneic rhabdomyosarcoma bearing WAG/Rij rats (22). Generally, Imaging of [^{18}F]FMISO uptake in xenograft-bearing mice demonstrated both high focal and more patchy distribution of the hypoxia PET tracer (32). These heterogeneous patterns of accumulation can be explained
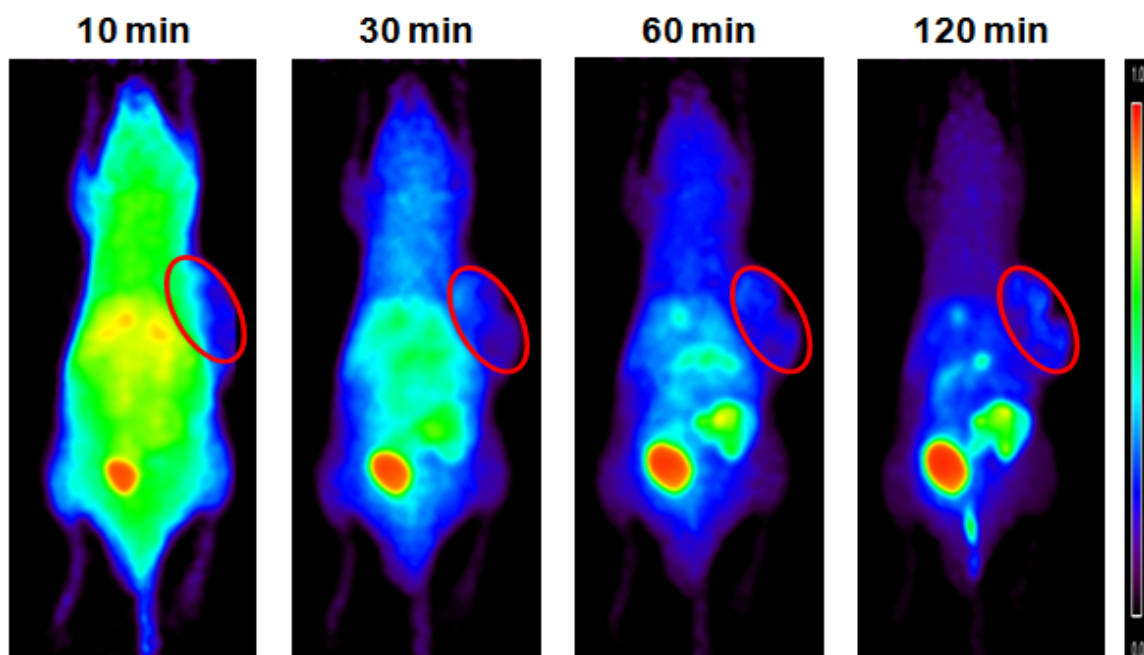
Figure 5. Small animal PET images of [^{18}F]FMISO (1.85 MBq/ 0.1 mL) in CT-26 xenografted mice after 10, 30, 60 and 120 min post-injection.

by the way vascular structures, responsible for the tracer influx and washout, are organized within the tumor (14). The tumor-to-non-tumor maximum SUV ratio of [^{18}F]FMISO (10 min: 1.07; 30 min: 1.20; 60 min: 1.42; and 120 min: 2.37) were also increased from 10 to 120 min post-injection. The SUVs for [^{18}F]FMISO showed statistically higher than [^{18}F]FAZA at 1 and 3 h post-injection in Walker 256 rat carcinoma tumors (11). This might be due to the higher lipophilicity of [^{18}F]FMISO (log = 2.6) than [^{18}F]FAZA (lop P = 1.1) (26) that allows [^{18}F]FMISO to penetrate the cell membrane more easily and to stay there even if unbound (11). PET using the 2-nitroimidazole [^{18}F]FMISO holds promise for the evaluation of tumor hypoxia at both global and local levels. Several alternative nitroimidazole derivatives have been developed to overcome some of the limitations of [^{18}F]FMISO such as nonspecific retention, metabolic conversion, and low partition coefficient, all leading to faster clearance properties (33).

Conclusion

We synthesized [^{18}F]FMISO using an automatic synthesis module with high radiochemical purity (>99%) in 60 min. Immunohistochemical staining of tumor hypoxia using pimonidazole hydrochloride showed the presence of hypoxia lesions in CT-26 tumor xenograft tissue. A biodistribution study in CT-26 xenografted mice showed that the increased tumor-to-muscle ratio and tumor-to-blood ratios from 10 to 120 min post-injection. In the PET study, [^{18}F]FMISO also showed increased tumor-to-muscle ratios from 10 to 120 min post-injection. In conclusion, this study demonstrates the feasibility and utility of [^{18}F]FMISO for imaging hypoxia in mouse colon cancer tumor models using small animal PET.

Acknowledgments

References

1. Lucignani G. PET imaging with hypoxia tracers: a must in radiation therapy. *Eur J Nucl Med Mol Imaging* 2008;35:838-842.
2. Lehtiö K, Eskola O, Viljanen T, Oikonen V, Grönroos T, Sillanmäki L, Grénman R, Minn H. Imaging perfusion and hypoxia with PET to predict radiotherapy response in head-and-neck cancer. *Int J Radiat Oncol Biol Phys* 2004;59:971-982.
3. Gambhir SS. Molecular imaging of cancer with positron emission tomography. *Nature Reviews Cancer* 2002;2:683-693.
4. Harry VN, Semple SI, Parkin DE, Gilbert FJ. Use of new imag-

ing techniques to predict tumour response to therapy. *Lancet Oncol* 2010;11:92-102.

5. Kelloff GJ, Hoffman JM, Johnson B, Scher HI, Siegel BA, Cheng EY, Cheson BD, O'Shaughnessy J, Guyton KZ, Mankoff DA. Progress and promise of FDG-PET imaging for cancer patient management and oncologic drug development. *Clin Ca Res* 2005;11:2785-2808.

6. Rajendran JG, Schwartz DL, O'Sullivan J, Peterson LM, Ng P, Scharnhorst J, Grierson JR, Krohn KA. Tumor hypoxia imaging with [F-18] fluoromisonidazole positron emission tomography in head and neck cancer. *Clin Ca Res* 2006;12:5435-5441.

7. Alauddin MM. Positron emission tomography (PET) imaging with 18F-based radiotracers. *Am J Nucl Med Mol Imaging* 2012;2:55.

8. Koh W-J, Rasey JS, Evans ML, Grierson JR, Lewellen TK, Graham MM, Krohn KA, Griffin TW. Imaging of hypoxia in human tumors with [F-18] fluoromisonidazole. *Int J Radiat Oncol Biol Phys* 1992;22:199-212.

9. Valk PE, Mathis CA, Prados MD, Gilbert JC, Budinger TF. Hypoxia in human gliomas: demonstration by PET with fluorine-18-fluoromisonidazole. *J Nucl Med* 1992;33:2133-2137.

10. Grönroos T, Eskola O, Lehtiö K, Minn H, Marjamäki P, Bergman J, Haaparanta M, Forsback S, Solin O. Pharmacokinetics of [^{18}F] FETNIM: a potential hypoxia marker for PET. *J Nucl Med* 2001;42:1397-1404.

11. Sorger D, Patt M, Kumar P, Wiebe LI, Barthel H, Seese A, Dannenberg C, Tannapfel A, Kluge R, Sabri O. [^{18}F] Fluoroazomycinarabinofuranoside (^{18}FAZA) and [^{18}F] Fluoromisonidazole (^{18}FMISO): a comparative study of their selective uptake in hypoxic cells and PET imaging in experimental rat tumors. *Nucl Med Biol* 2003;30:317-326.

12. Mahy P, De Bast M, Leveque P, Gillart J, Labar D, Marchand J, Grégoire V. Preclinical validation of the hypoxia tracer 2-(2-nitroimidazol-1-yl)-N-(3, 3, 3-[^{18}F] trifluoropropyl) acetamide, [^{18}F] EF3. *Eur J Nucl Med Mol Imaging* 2004;31:1263-1272.

13. Ziemer L, Evans S, Kachur A, Shuman A, Cardi C, Jenkins W, Karp J, Alavi A, Dolbier W, Koch C. Noninvasive imaging of tumor hypoxia in rats using the 2-nitroimidazole 18F-EF5. *Eur J Nucl Med Mol Imaging* 2003;30:259-266.

14. Dubois LJ, Lieuwes NG, Janssen MH, Peeters WJ, Windhorst AD, Walsh JC, Kolb HC, Öllers MC, Bussink J, van Dongen GA. Preclinical evaluation and validation of [^{18}F] HX4, a promising hypoxia marker for PET imaging. *Proc Nat Acad Sci* 2011;108:14620-14625.

15. Nunn A, Linder K, Strauss HW. Nitroimidazoles and imaging hypoxia. *Eur J Nucl Med* 1995;22:265-280.

16. Rauth A, Melo T, Misra V. Bioreductive therapies: an overview of drugs and their mechanisms of action. *Int J Radiat Oncol Biol Phys* 1998;42:755-762.

17. Takasawa M, Moustafa RR, Baron JC. Applications of nitroimidazole in vivo hypoxia imaging in ischemic stroke. *Stroke* 2008;39:1629-1637.

18. Kizaka-Kondoh S, Konse-Nagasawa H. Significance of nitroimidazole compounds and hypoxia-inducible factor-1 for imaging tumor hypoxia. *Ca Sci* 2009;100:1366-1373.

19. Hoigebazar L, Jeong JM. Hypoxia Imaging Agents Labeled with Positron Emitters. In: Theranostics, Gallium-68, and Other Radionuclides. edn.: Springer; 2013:285-299.

20. Kelada OJ, Carlson DJ. Molecular imaging of tumor hypoxia with positron emission tomography. *Radiat Res* 2014;181:335-349.

21. Tang G, Wang M, Tang X, Gan M, Luo L. Fully automated one-pot synthesis of [^{18}F] fluoromisonidazole. *Nucl Med Biol* 2005;32:553-558.

22. Dubois L, Landuyt W, Haustermans K, Dupont P, Bormans G, Vermaelen P, Flamen P, Verbeken E, Mortelmans L. Evaluation of hypoxia in an experimental rat tumour model by [^{18}F]Fluoromisonidazole PET and immunohistochemistry. *Br J Ca* 2004;91:1947-1954.

23. Bruehlmeier M, Roelcke U, Schubiger PA, Ametamey SM. Assessment of hypoxia and perfusion in human brain tumors using PET with 18F-fluoromisonidazole and ^{15}O-H$_2$O. *J Nucl Med* 2004;45:1851-1859.

24. Eschmann SM, Paulsen F, Reimold M, Dittmann H, Welz S, Reischl G, Machulla HJ, Bares R. Prognostic impact of hypoxia imaging with ^{18}F-misonidazole PET in non-small cell lung cancer and head and neck cancer before radiotherapy. *J Nucl Med* 2005;46:253-260.

25. Guadagno JV, Donnan GA, Markus R, Gillard JH, Baron JC. Imaging the ischaemic penumbra. *Curr Opin Neurol* 2004;17:61-67.

26. Markus R, Reutens DC, Kazui S, Read S, Wright P, Pearce DC, Tochon-Danguy HJ, Sachinidis JI, Donnan GA. Hypoxic tissue in ischaemic stroke: persistence and clinical consequences of spontaneous survival. *Brain* 2004;127(Pt 6):1427-1436.

27. Kumar P, Stypinski D, Xia H, McEwan AJB, Machulla HJ, Wiebe LI. Fluoroazomycin arabinoside (FAZA): synthesis, 2H and 3H-labelling and preliminary biological evaluation of a novel 2-nitroimidazole marker of tissue hypoxia. *J Label Compd Radiopharm* 1999;42:3-16.

28. Machulla HJ. Imaging of hypoxia: tracer developments, vol. 33: Springer Science & Business Media; 1999.

29. Oh SJ, Chi DY, Mosdzianowski C, Kim JY, Gil HS, Kang SH, Ryu JS, Moon DH. Fully automated synthesis of [^{18}F]fluoromisonidazole using a conventional [^{18}F]FDG module. *Nucl Med Biol* 2005;32:899-905.

30. Matsumoto K, Szajek L, Krishna MC, Cook JA, Seidel J, Grimes K, Carson J, Sowers AL, English S, Green MV et al. The influence of tumor oxygenation on hypoxia imaging in murine squamous cell carcinoma using [^{64}Cu]Cu-ATSM or [^{18}F]Fluoromisonidazole positron emission tomography. *Int J Oncol* 2007;30:873-881.

31. Hoigebazar L, Jeong JM, Lee JY, Shetty D, Yang BY, Lee YS, Lee DS, Chung JK, Lee MC. Syntheses of 2-Nitroimidazole Derivatives Conjugated with 1, 4, 7-Triazacyclononane-N, N′

-Diacetic Acid Labeled with F-18 Using an Aluminum Complex Method for Hypoxia Imaging. *J Med Chem* 2012; 55:3155-3162.

32. Troost EG, Laverman P, Kaanders JH, Philippens M, Lok J, Oyen WJ, van der Kogel AJ, Boerman OC, Bussink J. Imaging hypoxia after oxygenation-modification: Comparing [18F] FMISO autoradiography with pimonidazole immunohistochemistry in human xenograft tumors. *Radiother. Oncol.* 2006;80:157-164.

33. Krohn KA, Link JM, Mason RP. Molecular imaging of hypoxia. *J. Nucl. Med.* 2008;49 Suppl 2:129S-148S.

34. Wyss MT, Honer M, Schubiger PA, Ametamey SM. NanoPET imaging of [18F]fluoromisonidazole uptake in experimental mouse tumours. *Eur J Nucl Med Mol Imaging* 2006;33:311-318.

35. Piert M, Machulla HJ, Picchio M, Reischl G, Ziegler S, Kumar P, Wester HJ, Beck R, McEwan AJ, Wiebe LI, Schwaiger M. Hypoxia-specific tumor imaging with 18F-fluoroazomycin arabinoside. *J Nucl Med* 2005;46:106-113.

36. Gronroos T, Bentzen L, Marjamaki P, Murata R, Horsman MR, Keiding S, Eskola O, Haaparanta M, Minn H, Solin O. Comparison of the biodistribution of two hypoxia markers [18F]FETNIM and [18F]FMISO in an experimental mammary carcinoma. *Eur J Nucl Med Mol Imaging* 2004;31:513-520.

37. Cho H, Ackerstaff E, Carlin S, Lupu ME, Wang Y, Rizwan A, O'Donoghue J, Ling CC, Humm JL, Zanzonico PB, Koutcher JA. Noninvasive multimodality imaging of the tumor micro-environment: registered dynamic magnetic resonance imaging and positron emission tomography studies of a preclinical tumor model of tumor hypoxia. *Neoplasia (New York, NY)* 2009; 11:247-259, 242p following 259.

38. Sorensen M, Horsman MR, Cumming P, Munk OL, Keiding S. Effect of intratumoral heterogeneity in oxygenation status on FMISO PET, autoradiography, and electrode Po2 measurements in murine tumors. *Int J Radiat Oncol Biol Phys* 2005;62: 854-861.

39. Liu RS, Chou TK, Chang CH, Wu CY, Chang CW, Chang TJ, Wang SJ, Lin WJ, Wang HE. Biodistribution, pharmacokinetics and PET imaging of [18F]FMISO, [18F]FDG and [18F]FAc in a sarcoma- and inflammation-bearing mouse model. *Nucl Med Biol* 2009;36:305-312.

40. Tochon-Danguy HJ, Sachinidis JI, Chan F, Chan JG, Hall C, Cher L, Stylli S, Hill J, Kaye A, Scott AM. Imaging and quantitation of the hypoxic cell fraction of viable tumor in an animal model of intracerebral high grade glioma using [18F]fluoromisonidazole (FMISO). *Nucl Med Biol* 2002;29:191-197.

41. Riedl CC, Brader P, Zanzonico P, Reid V, Woo Y, Wen B, Ling CC, Hricak H, Fong Y, Humm JL. Tumor hypoxia imaging in orthotopic liver tumors and peritoneal metastasis: a comparative study featuring dynamic 18F-MISO and 124I-IAZG PET in the same study cohort. *Eur J Nucl Med Mol Imaging* 2008; 35:39-46.